A NONLINEAR LUMPED CIRCUIT MODEL FOR SCR

by

L. O. Chua and Y. W. Sing

Memorandum No. UCB/ERL M78/41

26 June 1978

ELECTRONICS RESEARCH LABORATORY

College of Engineering
University of California, Berkeley
94720

A NONLINEAR LUMPED CIRCUIT MODEL FOR SCR[†]

L. O. Chua and Y. W. Sing[††]

ABSTRACT

A nonlinear SCR circuit model made up of 6 lumped circuit elements (3 nonlinear capacitors and 3 nonlinear voltage-controlled current sources) is presented. The model can be used for simulating arbitrary SCR circuits under all operating conditions. In particular, it is capable of predicting all important dynamic effects such as turn-on and turn-off transients, dV/dt triggering, and the minimum commutation time phenomenon. Computer simulation results show that the model will correctly simulate all well-known triggering modes and turn-off mechanisms.

The model is based entirely upon the device's physical operating principles. Each element in the circuit model corresponds to an actual current component. In particular, carrier currents due to both diffusion and generation-recombination are included, in addition to the usual displacement current components across the 3 depletion layers.

[†]Research sponsored in part by the Office of Naval Research Contract N00014-76-0572 and the National Science Foundation Grant ENG77-22745.

[††]L. O. Chua is with the Department of Electrical Engineering and Computer Sciences and the Electronics Research Laboratory, University of California, Berkeley, California 94720

Y. W. Sing is with the Raytheon Company, Semiconductor Division, Mountain View, California 94042.

I. INTRODUCTION

Because of their high standard of reliability and performances, the silicon-controlled rectifiers (SCR) have been widely accepted in power-related circuit applications in industrial and military systems [1]. The design flexibilities provided by these devices have led to their applications in a broad range of operations. Indeed, the SCR is without any doubt the workhorse of modern power electronic circuits. Currently available SCR's are limited in their voltage and current ratings to about 3000 volts and 1800 amperes, respectively. However, laboratory models from such SCR manufacturers as General Electric, International Rectifier, Westinghouse, and RCA have pushed these limits to at least 5000 volts and 2000 amperes, while still maintaining fast switching time and high power efficiency.

Inspite of the widespread application of the SCR, circuits containing this device are usually designed by ad hoc methods. Failures are often avoided through wasteful over-design. For example, it is not unusual for power electronic circuit manufacturers to use a 100-watt SCR when 10 watts would suffice. This over-design was made because no realistic SCR circuit models are currently available for simulating the SCR circuits under continuous large-signal -- hence nonlinear -- operations.

Various SCR circuit models have been proposed in the literature [2-10]. These include the standard "two-transistor model," various digital models, and various piecewise-linear models. Unfortunately these models represent only gross approximations of the device's characteristics and fail to correctly predict the many important dynamic nonlinear effects which are crucial in any high-power transient simulation analysis. The reason why these models are unrealistic is because, except for the two-transistor model, they are derived from an intuitive "black box" approach with very little physical justifications. Our objective in this paper is to present a nonlinear lumped circuit model of the SCR which is derived entirely from device physics. Our approach is somewhat reminiscent of that which gives rise to the classic Ebers-Moll model for transistors [11].

Since the physical approach used in deriving our model include both diffusion and displacement current components, as well as components due to carrier generations and recombinations, our SCR circuit model is valid for both dc and dynamic operations and is independent of the external circuits. In other words, once the model parameters are identified for a given device, the circuit model is fixed, once and for all, and is valid under any mode of operation in any circuit environment.

Moreover, since each element in our model corresponds to an actual physical mechanism, much insights can be obtained by relating these mechanisms to the external circuit behavior.

Section II gives the basic circuit model along with the defining equations. Several equivalent circuit models are also given to allow their incorporation into circuit simulation programs which do not allow nonlinear controlled sources [9].

Section III contains many computer simulation examples using our model. These examples confirm our model's capability in simulating not only the nonlinear dc effects correctly, but also the various complicated dynamic nonlinear behaviors which are widely observed during triggering and other transient situations.

Finally, Section IV contains a physical derivation of our model, thereby providing a justification for its validity.

II. THE SCR CIRCUIT MODEL

The silicon-controlled rectifier (SCR) is a 3-terminal device made up of a p-n-p-n structure as shown in Fig. 1(a) along with its symbol in Fig. 1(b). The lumped circuit model for this device which will be derived and evaluated in the following sections is shown in Fig. 1(c). The model contains 6 elements; namely, 3 nonlinear capacitors and 3 nonlinear voltage-controlled current sources. The incremental capacitances describing the capacitors and the functions describing the controlled sources are completely specified by the following equations:

Nonlinear Capacitors

$$C_j(v_j) = C_{0j}[\psi_0 - v_j]^{-\frac{1}{m_j}} + \frac{I_{S_{ij}}\tau_j}{V_T} e^{v_j/V_T}, \quad j = 1,2,3 \tag{1}$$

Nonlinear Voltage Controlled Current Sources

$$f_A(v_1,v_2) = \left[(1+\gamma_1)I_{S_{11}} + I_{S_{15}}\right]\left[e^{v_1/V_T}-1\right] + I_{S_{21}}\left[e^{v_1/2V_T}-1\right] - I_{S_{12}}\left[e^{v_2/V_T}-1\right] \tag{2}$$

$$\begin{aligned} f_B(v_1,v_2,v_3) = {} & I_{S_{11}}\left[e^{v_1/V_T}-1\right] - \left[(1+\gamma_1)I_{S_{12}} + (1+\gamma_2)I_{S_{14}}\right]\left[e^{v_2/V_T}-1\right] \\ & - I_{S_{22}}\left[e^{v_2/2V_T}-1\right] + I_{S_{13}}\left[e^{v_3/V_T}-1\right] \end{aligned} \tag{3}$$

$$f_C(v_2,v_3) = -I_{S_{14}}\left[e^{v_2/V_T}-1\right] + \left[(1+\gamma_2)I_{S_{13}} + I_{S_{16}}\right]\left[e^{v_3/V_T}-1\right] + I_{S_{23}}\left[e^{v_3/2V_T}-1\right] \tag{4}$$

These equations are completely specified by the following 22 model parameters:

1. Physical parameters

   ψ_0 = junction contact potential (typically, $0.5 < \psi_0 < 1.2$ V)

   $V_T = kT/q$ (k = Boltzmann constant, q = electron charge, T = junction absolute temperature).

2. DC parameters

   $I_{S_{11}}, I_{S_{12}}, I_{S_{13}}, I_{S_{14}}, I_{S_{15}}, I_{S_{16}}$ (ideal saturation current component; typically, $10^{-16}\text{A} < I_{S_{1j}} < 10^{-10}\text{A}$)

   $I_{S_{21}}, I_{S_{22}}, I_{S_{23}}$ (nonlinear saturation current components; typically, $10^{-13}\text{A} < I_{S_{2j}} < 10^{-7}\text{A}$).

   γ_1, γ_2 (recombination factor for current components; typically $0.001 < \gamma_j < 1$).

3. AC parameters

   C_{01}, C_{02}, C_{03} (junction capacitance coefficient; typically, 0.5 pf $< C_{0j} <$ 4 pf).

   m_1, m_2, m_3 (junction grading coefficients; typically, $0.3 < m_j < 0.7$).

   τ_1, τ_2, τ_3 (minority carrier lifetimes; typically, 0.1 ns $< \tau_j <$ 20 ns).

The two physical parameters ψ_0 and V_T depend only on the device material and temperature and can be easily calculated from published data. The remaining parameters (11 DC and 9 AC parameters) must be determined by measurement and computer optimization techniques.

The circuit model shown in Fig. 1(c) contains 3 nonlinear controlled current sources which depend on two or three controlling voltages. While it would be highly desirable and quite easy to modify many existing computer simulation programs to allow these elements, it is also possible to use these programs directly by replacing the controlled sources in Fig. 1(c) by equivalent circuits via the transformation techniques described in [9]. In particular, the circuit model shown in Fig. 2 is equivalent to that of Fig. 1(c), provided the <u>nonlinear resistors</u> and the <u>linear controlled sources</u> are described as follow:

Nonlinear Resistors

$$R_1:\quad i_1 = I_1\left[e^{v_1/V_T}-1\right],\ I_1 \triangleq (1+\gamma_1)I_{S_{11}} + I_{S_{15}} \tag{5}$$

$$R_1':\quad i_1' = I_1'\left[e^{v_1/2V_T}-1\right],\ I_1' \triangleq I_{S_{21}} \tag{6}$$

$$R_2:\quad i_2 = I_2\left[e^{v_2/V_T}-1\right],\ I_2 \triangleq (1+\gamma_1)I_{S_{12}} + (1+\gamma_2)I_{S_{14}} \tag{7}$$

$$R_2':\quad i_2' = I_2'\left[e^{v_2/2V_T}-1\right],\ I_2' \triangleq I_{S_{22}} \tag{8}$$

$$R_3:\quad i_3 = I_3\left[e^{v_3/V_T}-1\right],\ I_3 \triangleq (1+\gamma_2)I_{S_{13}} + I_{S_{16}} \tag{9}$$

$$R_3':\quad i_3' = I_3'\left[e^{v_3/2V_T}-1\right],\ I_3' \triangleq I_{S_{23}} \tag{10}$$

Linear Current-Controlled Current Sources

Coefficient for the first controlled source:

$$k_1 \triangleq I_{S_{12}}/I_2 \tag{11}$$

coefficients for the second controlled source:[1]

$$k_2 \triangleq I_{S_{11}}/I_1,\ k_3 \triangleq I_{S_{13}}/I_3 \tag{12}$$

coefficient for the third controlled source

$$k_4 \triangleq I_{S_{14}}/I_2 \tag{13}$$

By substituting (5)-(13) into the KCL equations for Fig. 2 and comparing them with the corresponding KCL equations for Fig. 1(c), we found they are identical and hence the two models are equivalent. Observe that all 6 nonlinear resistors are characterized by an equation similar to that of a pn-junction diode. The 3 nonlinear capacitors are defined by (1) as in Fig. 1(c). Notice that the "thermal voltage" V_T is multiplied by 2 in (6), (8), and (10). We will see in Section IV that each element in this model corresponds to a physically generated current component in the device.

[1] If necessary, the second controlled source can be further decomposed into two controlled sources in parallel with each other.

From the circuit and system theoretic point of view, the SCR circuit model in Fig. 1(c) and Fig. 2 represents a current-controlled R-dynamic 2-port [12] characterized as follow:

State Equations:

$$\frac{dv_1}{dt} = \frac{I_A - f_A(v_1,v_2)}{C_1(v_1)} \triangleq f_1(v_1,v_2,v_3\,;I_A,I_G) \tag{14}$$

$$\frac{dv_2}{dt} = \frac{I_A - f_B(v_1,v_2,v_3)}{C_2(v_2)} \triangleq f_2(v_1,v_2,v_3;I_A,I_G) \tag{15}$$

$$\frac{dv_3}{dt} = \frac{I_A + I_G - f_C(v_2,v_3)}{C_3(v_3)} \triangleq f_3(v_1,v_2,v_3;I_A,I_G) \tag{16}$$

Output Equation:

$$V_{AC} = v_1 + v_2 + v_3 \triangleq g_1(v_1,v_2,v_3) \tag{17a}$$

$$V_G = v_3 \triangleq g_2(v_1,v_2,v_3) \tag{17b}$$

From the computer simulation point of view, one could just as well input the preceding equations instead of the circuit model provided the simulation program is sufficiently general to allow the user to describe the device directly in terms of a dynamical system, such as (14)-(17). This approach would be computationally more efficient because it obviates the need for the computer to derive the KVL and KCL equations associated with the circuit model.

III. COMPUTER SIMULATION EXAMPLES

Many examples have been simulated using our SCR circuit model under different circuit configurations and excitations. The following examples are particularly illuminating because they demonstrate the capabilities of our model in correctly predicting the many nonlinear dc and transient phenomena widely observed in practice.

Example 1. DC Anode V-I Characteristics

The static characteristics of the SCR are simulated using the circuit shown in Fig. 3(a) for 3 different values of gate currents. The 3 dc V-I curves shown in Fig. 3(b) are obtained with I_G = 0, 0.1, and 0.5 mA, respectively. The DC parameters chosen for this example are as follow:

$$I_{S_{11}} = I_{S_{12}} = I_{S_{13}} = I_{S_{14}} = I_{S_{15}} = I_{S_{16}} = 1 \times 10^{-11}\text{A}$$

$I_{S_{21}} = I_{S_{22}} = I_{S_{23}} = 1 \times 10^{-7}A$

$\gamma_1 = \gamma_2 = 0.01$

The AC parameters are of course irrelevant in this example. The results shown in Fig. 3(b) agree remarkably well with the typical manufacturer's characteristics of the SCR. Observe that the "holding current" [2] decreases from 5 to 3 mA as we increase the gate current from 0 to 0.5 mA. Observe also that the "peak turnover voltage" decreases from 1000 volts to 240 volts as we increase I_G from 0 to 0.5 mA.

Example 2. Gate V_G-I_G Characteristics

The gate characteristics of the SCR are simulated using the circuit shown in Fig. 4(a), where the SCR is biased by a fixed 20-volt battery in series with a 100 Ω resistance. A slowly-varying triangular gate voltage waveform $V_G(t)$ as shown in Fig. 4(b) is then applied and the resulting gate current $I_G(t)$ obtained by the computer using our SCR circuit model is shown in Fig. 4(c). The model parameters chosen for this example are:

1. Physical parameters

   $\psi_0 = 1$, $V_T = 26$ mV at 27°C.

2. DC parameters

   $I_{S_{11}} = I_{S_{12}} = I_{S_{13}} = I_{S_{14}} = I_{S_{15}} = I_{S_{16}} = 1 \times 10^{-14}A$

   $I_{S_{21}} = I_{S_{22}} = I_{S_{23}} = 5 \times 10^{-12}A$

   $\gamma_1 = \gamma_2 = 0.01$

3. AC parameters

   $C_{01} = 2$ pF, $C_{02} = 1$ pF, $C_{03} = 2$pF

   $m_1 = m_2 = m_3 = 0.5$

   $\tau_1 = 1$ ns, $\tau_2 = 10$ ns, $\tau_3 = 1$ ns

The waveforms shown in Figs. 4(b) and (c) can be explained physically as follow: Between points ① and ②, the gate voltage is insufficient to turn on the device, and the SCR is operating in its forward blocking state. At point ②, the threshold gate voltage V_G is reached, and the SCR turns on. Between points ③ and ④, the SCR remains in its "on-state" inspite of a decrease of V_G below its original threshold voltage. At point ④, the negative threshold voltage is reached and the SCR is turned off, and remains off until the cycle is repeated.

If we plot the relationship between $V_G(t)$ and $I_G(t)$ corresponding to the waveforms in Figs. 4(b) and (c), we would obtain the "Lissajous figure" shown in Fig. 4(d). Observe that this V_G-I_G characteristics is not a single-valued function. This well-known "multivalued" phenomenon [2] clearly distinguishes the SCR from the transistor in that the latter is basically "memoryless" at low frequencies, whereas the SCR exhibits important dynamic effects even at dc when the critical turn-on or turn-off point is reached. Since this transient behavior occurs whenever the SCR is being triggered on or off, any reasonable circuit model of the SCR must display this behavior.

Example 3. Anode Turn-on and Turn-Off Transients

Our next example simulates the anode voltage and current waveforms under various triggering mechanisms. The circuit simulated is shown in Fig. 5(a) where the anode voltage waveform V(t) shown in Fig. 5(b) and the gate triggering current waveform $I_G(t)$ shown in Fig. 5(c) are applied simultaneously. The resulting computer simulated waveform for the anode current I(t) is shown in Fig. 5(d), where the same model parameters chosen in Example 2 are used. The waveforms V(t) and $I_G(t)$ have been carefully chosen here in order to demonstrate the various mechanisms by which an SCR may be turned on or off. The various instants of time of particular interest are labelled in Figs. 5(b), (c), and (d). During the time interval between ① and ②, the anode voltage V(t), though increasing with time, is too small (V is less than threshold) and too slow (dV/dt is less than critical rate) to turn on the device so that the SCR is operating in its "forward blocking state," where the anode current $I(t) \approx 0$. At point ② where $V \approx 1000$ Volts (note the break in the waveform indicating a change of scale), the triggering anode threshold voltage is reached and the device turns on with a large anode current I(t) flowing between points ② and ③, and the SCR is operating in its forward conducting state. AT point ③, where V(t) reaches a peak value of 1200 Volts, the anode voltage decreases monotonically at a slow rate until V(t) becomes zero at point ④ and remains at zero until point ⑤. The anode current I(t) decreases with V(t) from point ③ to point ④ while the SCR remains in its forward conducting state (even though V(t) has decreased below the original triggering threshold value at point ②). The SCR turns off somewhere between points ④ and ⑤ where V(t) = 0, and remains in its forward blocking state while we increase V(t) again from point ⑤ to ⑥. At point ⑥, V(t) is increased rapidly with dV/dt >> 0 and the SCR turns on with an increasing anode current I(t), even though the magnitude (≈100 Volts) of V(t) is still far below the triggering threshold value at point ②. This clearly demonstrates the dV/dt triggering mechanism widely reported in the literature [1-2]. The SCR remains in it forward conducting state during the time interval between points ⑥ and ⑦ even though V(t) is decreased rapidly (dV/dt << 0). At point ⑦, we apply a negative gate triggering current, thereby turning off the device as indicated by an initial rise and subsequent decay to zero in the anode current I(t). The SCR remains in its forward blocking state until point ⑧ where a positive gate triggering current is applied, thereby turning on the device as indicated by the sudden increase in I(t). Observe that even though the anode voltage V(t) is decreased to zero from points ⑧ to ⑨, the device remains in its forward conducting state as demonstrated by the slight increase in the anode current I(t) due to a corresponding slight increase in the anode voltage V(t) at and beyond point ⑨. This phenomenon is usually referred to in the literature as a "failure to turn off due to insufficient commutation time" [1-2].

This example demonstrates that our model is indeed capable of predicting the various distinct physical mechanisms for turning an SCR on or off. It is important to understand that all of the complicated transient behaviors depicted in Fig. 5 are due to nonlinear dynamic effects and could not have been properly predicted by a dc model, or even a digital model under arbitrary loading conditions. Indeed, any realistic SCR circuit model must be capable of mimicking these mechanisms to be of any value in transient simulation.

Example 4. An SCR Circuit with an Inductive Load

The preceding examples involve only a resistor-battery external circuit. For our last examples, consider the SCR series RL circuit shown in Fig. 6(a). The series resistor R is included merely to sense the current through the SCR, and is intentionally set nearly equal to zero in order to emphasize the loading effects due to the inductor. The circuit is driven by a sinusoidal voltage waveform $v_s(t)$ as shown in Fig. 6(b) and a periodic gate triggering pulse train $V_G(t)$ as shown in Fig. 6(c). Using the same model parameters as those of Example 2, we obtained the computer-simulated output current waveform I(t) in Fig. 6(d). Again, the phase relationship and the output waveshape of I(t) agree remarkably well with well-known published results.

IV. DERIVATION OF THE SCR CIRCUIT MODEL

Although the examples in Section III all tend to support the accuracy of our model, it remains for us to give the detailed derivations of this model in terms of device physics.

Consider the one-dimensional pnpn SCR structure shown in Fig. 7(a) along with a typical doping concentration as shown in Fig. 7(b). If we apply a forward-biased voltage V_{AC} across the device, the mobile carriers will be depleted from the junctions, leaving the depletion layers as shown in Fig. 7(c). Now the anode current I_A is composed of a displacement current I_{Ad} and a carrier current I_{Ac} made up of hole and electron currents injected from junction 1; namely,

$$I_A = I_{Ad} + I_{Ac} = I_{Ad} + I_{Ah} + I_{Ae} \tag{18}$$

where I_{Ah} and I_{Ae} denote the hole and electron currents, respectively in the P_1 region. Similarly, the cathode current I_C is composed of a displacement current I_{Cd} and a carrier current I_{Cc} made up of hole and electrons injection from junction 3:

$$I_C = I_{Cd} + I_{Cc} = I_{Cd} + I_{Ch} + I_{Ce} \tag{19}$$

where I_{Ch} and I_{Ce} denote the hole and electron currents, respectively in the N_2 region.

Finally, at junction 2, we have

$$\text{Total cross-section current} = I_A = I_{Bd} + I_{Bc} \tag{20}$$

where I_{Bd} and I_{Bc} denote the displacement and carrier currents crossing junction 2, respectively. Now, applying KCL across the cut set formed by the 3 external terminals, we obtain

$$I_C = I_A + I_G \tag{21}$$

where I_G is the gate current. Observe now that (18), (19), (20), and (21) are satisfied precisely by the circuit model shown in Fig. 1(c). Hence, we only need to show that each of the current components in (18)-(21) is governed by the equations defining the elements in the model.

The 3 displacement currents I_{Ad}, I_{Bd}, and I_{Cd} are governed by well-known laws between the charge and voltage across each depletion layer and can be modeled by 3 nonlinear junction capacitors whose incremental capacitances $C_1(v_1)$, $C_2(v_2)$, and $C_3(v_3)$ are precisely those defined by (1). The carrier currents I_{Ac}, I_{Bc}, and I_{Cc} are made up of a diffusion current component and a generation-recombination current component in the depletion region. These components are shown symbolically in Fig. 8, where the solid lines indicate the component current flow due to holes, and the dotted lines indicate the component current flow due to electrons. These components are defined below along with its relationship in terms of the junction voltages as derived in the Appendix:

A. Diffusion current components:[2]

$I_{d_1} = I_{S_{11}}\left[e^{v_1/V_T}-1\right]$ = <u>holes</u> injected from J_1 into N_1 and which diffused across N_1

$I_{d_2} = I_{S_{12}}\left[e^{v_2/V_T}-1\right]$ = <u>holes</u> injected from J_2 into N_1 and which diffused across N_1

$I_{d_3} = I_{S_{13}}\left[e^{v_3/V_T}-1\right]$ = <u>electrons</u> injected from J_3 into P_2 and which diffused across P_2.

$I_{d_4} = I_{S_{14}}\left[e^{v_2/V_T}-1\right]$ = <u>electrons</u> injected from J_2 into P_2 and which diffused across P_2.

$I_{d_5} = I_{S_{15}}\left[e^{v_1/V_T}-1\right]$ = <u>electrons</u> injected from J_1 into P_1 and which diffused across P_1.

$I_{d_6} = I_{S_{16}}\left[e^{v_3/V_T}-1\right]$ = <u>holes</u> injected from J_3 into N_2 and which diffused across N_2.

The parameters $I_{S_{11}}$, $I_{S_{12}}$, $I_{S_{13}}$, $I_{S_{14}}$, $I_{S_{15}}$, and $I_{S_{16}}$ are constants which depend on the intrinsic parameters of the device.

B. Recombination current components <u>outside</u> the depletion region:[3]

$I_{ro_1} = \gamma_1 I_{d_1}$ = fraction of <u>holes</u> injected from J_1 which recombines with electrons in N_1.

$I_{ro_2} = \gamma_1 I_{d_2}$ = fraction of <u>holes</u> injected from J_2 which recombines with electrons in N_1.

$I_{ro_3} = \gamma_2 I_{d_3}$ = fraction of <u>electrons</u> injected from J_3 which recombines with holes in P_2.

$I_{ro_4} = \gamma_2 I_{d_4}$ = fraction of <u>electrons</u> injected from J_2 which recombines with holes in P_2.

The parameters γ_1 and γ_2 are the minority carrier recombination coefficients in N_1 and P_2, respectively.

---

[2]The double subscript d_j" in I_{d_j} denotes the <u>D</u>iffusion current component in N_j or P_j.

[3]The triple subscripts "ro_j" in I_{ro_j} denotes the <u>R</u>ecombination current component <u>O</u>utside the depletion region <u>j</u>.

C. Recombination Current Components inside the Depletion Region:[4]

$I_{ri_1} = I_{S_{21}}\left[e^{v_1/2V_T}-1\right]$ = current component due to holes which recombine with electrons in J_1.

$I_{ri_2} = I_{S_{22}}\left[e^{v_2/2V_T}-1\right]$ = current component due to holes which recombine with electrons in J_2.

$I_{ri_3} = I_{S_{23}}\left[e^{v_3/2V_T}-1\right]$ = current component due to electrons which recombine with holes in J_3.

The parameters $I_{S_{21}}$, $I_{S_{22}}$, and $I_{S_{23}}$ are constants which depend on the intrinsic parameters of the device. It is important to note that unlike the expressions defining the current component I_{d_j}, the above expressions have a factor "2" multiplying the thermal voltage V_T. Roughly speaking, the factor 2 comes from the fact that while the region outside of the depletion layer contains only majority carriers, the region inside the depletion layer contains both majority and minority carriers in nearly equal numbers.

Referring now to Fig. 8, we obtain immediately,

$$I_{Ah} = \left\{\begin{array}{l}\text{hole current injected through}\\ \text{Junction 1 into } N_1 \text{ and which}\\ \text{diffused across } N_1 \text{ and}\\ \text{collection at Junction 2}\end{array}\right\} + \left\{\begin{array}{l}\text{hole current injected through}\\ \text{Junction 1 into } N_1 \text{ and which}\\ \text{recombined with electrons in}\\ N_1\end{array}\right\}$$

$$+\left\{\begin{array}{l}\text{hole current which recombined}\\ \text{with electrons in Junction}\\ J_1\end{array}\right\} - \left\{\begin{array}{l}\text{hole current injected through}\\ \text{junction 2 into } N_1 \text{ and which}\\ \text{diffused across } N_1 \text{ and collected}\\ \text{at Junction 1}\end{array}\right\}$$

$$= I_{d_1} + I_{ro_1} + I_{ri_1} - I_{d_2}$$

$$= I_{S_{11}}\left[e^{v_1/V_T}-1\right] + \gamma_1 I_{S_{11}}\left[e^{v_1/V_T}-1\right] + I_{S_{21}}\left[e^{v_2/2V_T}-1\right] - I_{S_{12}}\left[e^{v_2/V_T}-1\right] \qquad (22)$$

[4]The triple subscript, "ri_j" in I_{ri_j} denotes the Recombination current component Inside the depletion region j.

$$I_{Ae} = \left\{\begin{array}{l}\text{electron current}\\ \text{injected through Junction 1}\\ \text{into } P_1\end{array}\right\} = I_{d_5} = I_{S_{15}}\left[e^{v_1/V_T}-1\right] \tag{23}$$

$$I_{B_c} = \left\{\begin{array}{l}\text{hole current injected}\\ \text{from Junction 2}\\ \text{into } P_2\end{array}\right\} + \left\{\begin{array}{l}\text{current generated}\\ \text{in Junction 2}\end{array}\right\} + \left\{\begin{array}{l}\text{electron current}\\ \text{injected from}\\ \text{Junction 2 into } N_1\end{array}\right\}$$

$$= \left\{I_{d_1} - I_{d_2} - I_{ro_2} - I_{ri_2}\right\} + \left\{I_{ri_2}\right\} + \left\{I_{d_3} - I_{d_4} - I_{ro_4} - I_{ri_2}\right\}$$

$$= I_{d_1} - I_{d_2} - I_{ro_2} + I_{d_3} - I_{d_4} - I_{ri_2} - I_{ro_4}$$

$$\begin{aligned} &= I_{S_{11}}\left[e^{v_1/V_T}-1\right] - I_{S_{12}}\left[e^{v_2/V_T}-1\right] - \gamma_1 I_{S_{12}}\left[e^{v_2/V_T}-1\right] + I_{S_{13}}\left[e^{v_3/V_T}-1\right] \\ &\quad - I_{S_{14}}\left[e^{v_2/V_T}-1\right] - I_{S_{22}}\left[e^{v_2/2V_T}-1\right] - \gamma_2 I_{S_{14}}\left[e^{v_2/V_T}-1\right] \end{aligned} \tag{24}$$

$$I_{C_e} = \left\{\begin{array}{l}\text{electron current injected}\\ \text{through Junction 3 into}\\ P_2 \text{ and which diffused}\\ \text{across } P_2 \text{ and collected}\\ \text{at Junction 2}\end{array}\right\} + \left\{\begin{array}{l}\text{hole current injected}\\ \text{through Junction 3 into}\\ P_2 \text{ and which recombined}\\ \text{with holes in } P_2\end{array}\right\}$$

$$+ \left\{\begin{array}{l}\text{electron current which}\\ \text{recombine with}\\ \text{holes in Junction 3}\end{array}\right\} - \left\{\begin{array}{l}\text{electron current injected through}\\ \text{Junction 2 into } P_2 \text{ and which diffused}\\ \text{across } P_2 \text{ and collected at } J_3\end{array}\right\}$$

$$= I_{d_3} + I_{ro_3} + I_{ri_3} - I_{d_4}$$

$$= I_{S_{13}}\left[e^{v_3/V_T}-1\right] + \gamma_2 I_{S_{13}}\left[e^{v_3/V_T}-1\right] + I_{S_{23}}\left[e^{v_3/2V_T}-1\right] - I_{S_{14}}\left[e^{v_2/V_T}-1\right] \tag{25}$$

$$I_{Ch} = \left\{\begin{array}{l}\text{hole current} \\ \text{injected from} \\ \text{Junction 3 into } N_2\end{array}\right\} = I_{d_6} = I_{S_{16}}\left[e^{v_3/V_T}-1\right] \tag{26}$$

Finally, if we substitute (22)-(23) into (18), (24) into (20), and (25)-(26) into (19), we would obtain the element characteristics specified in (1)-(4).

APPENDIX: Derivation of Carrier Current Components

The derivations in this Appendix follow standard techniques [2,13] and are given here only for the reader's convenience.

1. Diffusion current components:

Consider the typical minority carrier concentration profile shown in Fig. A.1, where we have assumed the width of the depletion layers to be negligible. Assuming the electric field outside the depletion region is also negligible, the conducting electron current in p_1 is given by the diffusion equation

$$I_{n_p} = Aq\, D_n \frac{dn_p}{dx} \tag{A.1}$$

where A is the area of the device, q is the electron charge, D_n is the electron diffusion coefficient, and n_p is the electron concentration as a function of x, where x = 0 is located at the right boundary of the P_1 layer. Substituting (A.1) into the continuity equation, we obtain

$$\frac{d^2 n_p}{dx^2} = \frac{n_p - n_{p_o}}{D_n \tau_n} = \frac{n_p - n_{p_o}}{L_n^2} \tag{A.2}$$

where $L_n \triangleq \sqrt{D_n \tau_n}$ is the electron diffusion length, and τ_n is the minority carrier life time in the P_1 region. The general solution of (A.1) is:

$$n_p(x) - n_{p_o} = k_1 e^{x/L_n} + k_2 e^{-x/L_n} \tag{A.3}$$

Applying the boundary conditions

$$x = 0,\ n_p(0) = n_{p_1}(0) = \frac{n_i^2}{N_{p_1}} e^{v_1/V_T} \tag{A.4}$$

$$x = w_{p_1},\ n_p(w_{p_1}) = n_{p_{01}} = \frac{n_i^2}{N_{p_1}} \tag{A.5}$$

where n_i is the intrinsic electron concentration and N_{p_i} is the impurity concentration in the P_1 layer, we obtain the solution.

$$n_{p_1}(x) - n_{p_{01}} = \frac{n_i^2}{N_{p_1}} \left[\frac{\sinh\left(\frac{x - W_{p_1}}{L_n}\right)}{\sinh\left(\frac{W_{p_1}}{L_n}\right)} \right] \left[e^{v_1/V_T} - 1 \right] \tag{A.6}$$

Now referring to the current component diagram in Fig. 8, we have:

$$I_{d_5} = \left\{ \begin{array}{l} \text{electron current injected} \\ \text{from Junction 1 into } P_1 \end{array} \right\} = qD_n \left. \frac{dn_p}{dx} \right|_{x=0}$$

$$= \frac{AqD_n n_i^2}{N_{p_1} L_n} \coth\left(\frac{W_{p_1}}{L_n}\right) \left[e^{v_1/V_T} - 1 \right] = I_{S_{15}} \left[e^{v_1/V_T} - 1 \right] \tag{A.7}$$

Under the same assumption, the conducting hole current in N_2 is given by the diffusion equation

$$I_{p_n} = AqD_p \frac{dp_n}{dy} \tag{A.8}$$

where D_p is the hole diffusion coefficient, and p_n is the hole concentration as a function of y, where y = 0 is located at the left boundary of the N_2 layer. Substituting (A.8) into the continuity equation

$$\frac{d^2 p_n}{dy^2} = \frac{p_n - p_{n_o}}{D_p \tau_p} = \frac{p_n - p_{n_o}}{L_p^2} \tag{A.9}$$

where $L_p = \sqrt{D_p \tau_p}$ is the electron diffusion length, and τ_p is the minority carrier life time in the N_2 region. The general solution of (A.8) is:

$$p_n(y) - p_{n_o} = K_1 e^{y/L_p} + K_2 e^{-y/L_p} \tag{A.10}$$

Applying the boundary conditions

$$y = 0 \ : \ p_n(0) = p_{n_2}(0) = \frac{n_i^2}{P_{n_2}} e^{v_3/V_T} \tag{A.11}$$

$$y = w_{n_2} : p_n(w_{n_2}) = p_{n_{02}} = \frac{n_i^2}{P_{n_2}} \tag{A.12}$$

where P_{n_2} is the impurity concentration in the N_2 layer, we obtain the solution

$$p_n(y) - p_{n_{02}} = \frac{n_i^2}{P_{n_2}} = \left[\frac{\sinh\left(\frac{y - w_{n_2}}{L_p}\right)}{\sinh\left(\frac{w_{n_2}}{L_p}\right)} \right] \left[e^{v_3/V_T} - 1 \right] \tag{A.13}$$

Referring to the current component diagram in Fig. 8, we have:

$$I_{d_6} = \left\{\begin{matrix}\text{electron current injected}\\ \text{from Junction 3 into } N_2\end{matrix}\right\} = qD_p \left.\frac{dp_n}{dy}\right|_{y=0}$$

$$= \frac{AqD_p n_i^2}{P_{n_2} L_p} \coth\left(\frac{w_{n_2}}{L_p}\right)\left[e^{v_3/V_T}-1\right] = I_{S_{16}}\left[e^{v_3/V_T}-1\right] \quad (A.14)$$

Let us solve next for the diffusion equation

$$\frac{d^2 p_n}{dx'^2} = \frac{p_n - p_{n_o}}{D_p \tau_p}$$

in the N_1 layer, where D_p is the hole diffusion coefficient, and τ_p is the minority carrier life time in the N_1 region. Note that the space variable x' in Fig. A.1 is now measured from the left boundary at Junction 1. The solution to (A.14) with the boundary conditions

$$x' = 0, \quad p_n(0) = \frac{n_i^2}{N_{n_1}} e^{v_1/V_T} \quad (A.15)$$

$$x' = w_{n_1}, \quad p_n(w_{n_1}) = \frac{n_i^2}{N_{n_1}} e^{v_2/V_T} \quad (A.16)$$

is given by

$$p_n(x) - p_{n_o} = -\frac{n_i^2}{N_{n_1}} \operatorname{csch}\left(\frac{w_{n_1}}{L_p}\right)\left\{\sinh\left(\frac{x'-w_{n_1}}{L_p}\right)\left[e^{v_1/V_T}-1\right] - \sinh\left(\frac{x'}{L_p}\right)\left[e^{v_2/V_T}-1\right]\right\} \quad (A.17)$$

Now the hole current at x' = 0 can be obtained by solving the diffusion equation and using (A.17):

$$I_p\Big|_{x'=0} = -AqD_p \left.\frac{dp}{dx'}\right|_{x'=0}$$

$$= \frac{AqD_p n_i^2}{L_p N_{n_1}} \coth \frac{w_{n_1}}{L_p}\left[e^{v_1/V_T}-1\right] - \frac{AqD_p n_i^2}{L_p N_{n_1}} \operatorname{csch}\left(\frac{w_{n_1}}{L_p}\right)\left[e^{v_2/V_T}-1\right]$$

$$= \left\{\begin{matrix}\text{hole current injected}\\ \text{from Junction 1 into } N_1\end{matrix}\right\} - \left\{\begin{matrix}\text{hole current injected from Junction 2}\\ \text{into } N_1 \text{ and which diffused across}\\ N_1 \text{ and collected at Junction 1}\end{matrix}\right\}$$

$$= \begin{Bmatrix} \text{hole current injected} \\ \text{from Junction 1 into } N_1 \end{Bmatrix} - I_{d_2} \tag{A.18}$$

where

$$I_{d_2} \triangleq I_{S_{12}} \left[e^{v_2/V_T} - 1 \right] = \frac{AqD_p n_i^2}{L_p N_{n_1}} \operatorname{csch}\left(\frac{w_{n_1}}{L_p} \right) \left[e^{v_2/V_T} - 1 \right] \tag{A.19}$$

substituting (A.17) into the diffusion equation at $x' = w_{n_1}$. We obtain,

$$\begin{aligned} I_{p_{x'=w_{n_1}}} &= -AqD_p \left. \frac{dp}{dx'} \right|_{x'=w_{n_1}} \\ &= \frac{AqD_p n_i^2}{L_p N_{n_1}} \operatorname{csch}\left(\frac{w_{n_1}}{L_p} \right) \left[e^{v_1/V_T} - 1 \right] \\ &\quad - \frac{AqD_p n_i^2}{L_p N_{n_1}} \coth\left(\frac{w_{n_1}}{L_p} \right) \left[e^{v_2/V_T} - 1 \right] \\ &= I_{d_1} - \frac{AqD_p n_i^2}{L_p N_{n_1}} \coth\left(\frac{w_{n_1}}{L_p} \right) \left[e^{v_2/V_T} - 1 \right] \\ &= I_{d_1} - \begin{Bmatrix} \text{hole current injected from} \\ \text{Junction 2 into } N_1 \end{Bmatrix} \end{aligned}$$

where

$$I_{d_1} \triangleq I_{S_{11}} \left[e^{v_1/V_T} - 1 \right] = \frac{AqD_p n_i^2}{L_p N_{n_1}} \operatorname{csch}\left(\frac{w_{n_1}}{L_p} \right) \left[e^{v_1/V_T} - 1 \right] \tag{A.20}$$

Now

$$I_{ro_1} \triangleq \gamma_1 I_{d_1} = \begin{Bmatrix} \text{current due to holes injected from Junction 1} \\ \text{into } N_1 \text{ and which recombined with} \\ \text{electrons} \end{Bmatrix} \tag{A.21}$$

$$= \begin{Bmatrix} \text{holes injected from} \\ \text{Junction 1 into } N_1 \end{Bmatrix} - \begin{Bmatrix} \text{holes injected from Junction 1} \\ \text{into } N_1 \text{ and which diffused across} \\ N_1 \text{ and collected at Junction 2} \end{Bmatrix}$$

$$= \frac{AqD_p n_i^2}{L_p N_{n_1}} \coth\left(\frac{w_{n_1}}{L_p}\right) \left[e^{v_1/V_T} - 1\right] - I_{d_1}$$

$$= \left\{\frac{AqD_p n_i^2}{L_p N_{n_1}} \coth\left(\frac{w_{n_1}}{L_p}\right) \left[e^{v_1/V_T} - 1\right] \Big/ I_{d_1} - 1\right\} I_{d_1}$$

$$= \left\{\frac{AqD_p n_i^2}{L_p N_{n_1}} \coth\left(\frac{w_{n_1}}{L_p}\right) \left[e^{v_1/V_T} - 1\right] \Big/ \frac{AqD_p n_i^2}{L_p N_{n_1}} \operatorname{csch}\left(\frac{w_{n_1}}{L_p}\right) \left[e^{v_1/V_T} - 1\right] - 1\right\} I_{d_1}$$

$$= \left[\cosh\left(\frac{w_{n_1}}{L_p}\right) - 1\right] I_{d_1} \tag{A.22}$$

Comparing (A.22) with (A.21), we obtain

$$\gamma_1 = \cosh\left(\frac{w_{n_1}}{L_p}\right) - 1 \tag{A.23}$$

Let us solve next the diffusion equation

$$\frac{d^2 n_p}{dy'^2} = \frac{n_p - n_{p_o}}{D_n \tau_n} \tag{A.24}$$

in the P_2 layer, where the variable y' in Fig. A.1 is measured from the right boundary at P_2. The solution to (A.24) with the boundary conditions

$$y' = 0 \quad : \quad n_p(0) = \frac{n_i^2}{P_{p_2}} e^{v_3/V_T} \tag{A.25}$$

$$y' = w_{p_2} \quad : \quad n_p(w_{p_2}) = \frac{n_i^2}{P_{p_2}} e^{v_2/V_T} \tag{A.26}$$

is given by

$$n_p(y') - n_{p_o} = -\frac{n_i^2}{P_{p_2}} \operatorname{csch}\left(\frac{w_{p_2}}{L_n}\right)\left\{\sinh\left(\frac{y'-w_{p_2}}{L_n}\right)\left[e^{v_3/V_T} - 1\right] - \sinh\left(\frac{y'}{L_n}\right)\left[e^{v_2/V_T} - 1\right]\right\} \tag{A.27}$$

Now the hole current in y' = 0 can be obtained by solving the diffusion equation and using (A.26):

$$I_n\Big|_{y'=0} = AqD_n \frac{dn}{dy'}\Big|_{y'=0}$$

$$= \frac{AqD_n n_i^2}{L_n P_{p_2}} \coth\left(\frac{w_{p_2}}{L_n}\right)\left[e^{v_3/V_T}-1\right] - \frac{AqD_n n_i^2}{L_n P_{p_2}} \operatorname{csch}\left(\frac{w_{p_2}}{L_n}\right)\left[e^{v_2/V_T}-1\right]$$

$$= \left\{\begin{matrix}\text{electron current injected} \\ \text{from Junction 3 into } P_2\end{matrix}\right\} - \left\{\begin{matrix}\text{electron current injected} \\ \text{from Junction 2 into } P_2 \text{ and which} \\ \text{diffused across } p_2 \text{ and collected} \\ \text{at Junction 3}\end{matrix}\right\}$$

$$= \left\{\begin{matrix}\text{electron current injected} \\ \text{from Junction 3 into } P_2\end{matrix}\right\} - I_{d_4}$$

where

$$I_{d_4} \triangleq I_{S_{14}} \left[e^{v_2/V_T}-1\right] = \frac{AqD_n n_i^2}{L_n P_{p_2}} \operatorname{csch}\left(\frac{w_{p_2}}{L_n}\right) \left[e^{v_3/V_T}-1\right] \tag{A.28}$$

Substituting (A.28) into the diffusion equation at $x' = w_{p_2}$, we obtain,

$$I_n\Big|_{y'=w_{p_2}} = AqD_n \frac{dn}{dy'}\Big|_{x'=w_{p_2}}$$

$$= \frac{AqD_n n_i^2}{L_n P_{p_2}} \operatorname{csch}\left(\frac{w_{p_2}}{L_n}\right)\left[e^{v_3/V_T}-1\right] - \frac{AqD_n n_i^2}{L_n P_{p_2}} \coth\left(\frac{w_{p_2}}{L_n}\right)\left[e^{v_2/V_T}-1\right]$$

$$= I_{d_3} - \frac{AqD_n n_i^2}{L_n P_{p_2}} \coth\left(\frac{w_{p_2}}{L_n}\right) \left[e^{v_2/V_T}-1\right]$$

$$= I_{d_3} - \left\{\begin{matrix}\text{electron current injected from} \\ \text{Junction 2 into } p_2\end{matrix}\right\}$$

where

$$I_{d_3} \triangleq I_{S_{13}} \left[e^{v_3/V_T}-1\right] \triangleq \frac{AqD_n n_i^2}{L_n P_{p_2}} \operatorname{csch}\left(\frac{w_{p_2}}{L_n}\right)\left[e^{v_3/V_T}-1\right] \tag{A.29}$$

Now

$$I_{ro_2} \triangleq \gamma_2 I_{d_3} = \left\{\begin{matrix}\text{current due to electrons injected from} \\ \text{Junction 3 into } P_2 \text{ and which recombined} \\ \text{with electrons}\end{matrix}\right\} \tag{A.30}$$

$$= \left\{\begin{matrix}\text{electrons injected from} \\ \text{3 into } P_2\end{matrix}\right\} - \left\{\begin{matrix}\text{electrons injected from Junction 3} \\ \text{into } P_2 \text{ and which diffused across} \\ P_2 \text{ and collected at Junction 2}\end{matrix}\right\}$$

$$= \frac{AqD_n n_i^2}{L_n P_{p_2}} \coth\left(\frac{w_{p_2}}{L_n}\right)\left[e^{v_3/V_T}-1\right] - I_{d_3}$$

$$= \left\{\frac{AqD_n n_i^2}{L_n P_{p_2}} \coth\left(\frac{w_{p_2}}{L_n}\right)\left[e^{v_3/V_T}-1\right] \Big/ \frac{AqD_n n_i^2}{L_n P_{p_2}} \operatorname{csch}\left(\frac{w_{p_2}}{L_n}\right)\left[e^{v_3/V_T}-1\right] - 1\right\} I_{d_3}$$

$$\triangleq \left[\cosh\left(\frac{w_{p_2}}{L_n}\right) -1\right] I_{d_3} \tag{A.31}$$

Comparing (A.30) with (A.29), we obtain

$$\gamma_2 = \left[\cosh\left(\frac{w_{p_2}}{L_n}\right) - 1\right] \tag{A.32}$$

2. Generation and Recombination current components in the depletion region

It can be shown that the carrier generation rate is given by [2]

$$U = \sigma v_{th} N_t \left[\frac{pn-n_i^2}{n+p+2n_i}\right] \tag{A.33}$$

where σ is the carrier capture cross section, v_{th} is the carrier thermal velocity, and N_t is the trap density. Assuming the hole and electron concentrations are equal in the depletion layer, (A.33) becomes

$$U = \sigma v_{th} N_t \left\{\frac{n_i^2\left[e^{v_F/V_T}-1\right]}{2n_i\left[e^{v_F/V_T}-1\right]}\right\} = \frac{\sigma v_{th} N_t}{2}\left[e^{v_F/2V_T}-1\right] \tag{A.34}$$

where v_F is the forward voltage across the depletion layer. It follows from (A.34) that the generation-recombination current in the depeletion layer is given by

$$I = qA\int_0^{w_d} U dx = \frac{qAw_d \sigma v_{th} N_t}{2}\left[e^{v_F/2V_T}-1\right] \tag{A.35}$$

where A is the cross section area and w_d is the width of the depletion layer. Applying (A.33) to Junctions 1, 2, and 3, respectively, we obtain

$$I_{ri_1} = I_{S_{21}}\left[e^{v_1/2V_T}-1\right] \tag{A.36}$$

$$I_{ri_2} = I_{S_{22}}\left[e^{v_2/2V_T}-1\right] \tag{A.37}$$

$$I_{ri_3} = I_{S_{23}}\left[e^{v_3/2V_T}-1\right] \tag{A.38}$$

REFERENCES

[1] Harnden, J.D. and Golden, F.B. (editors), Power Semiconductor Applications, Vols. 1 and 2, IEEE Press, New York, 1972.

[2] Gentry, F.E., F.W. Gutzwiller, N. Holonyak, Jr., and E.E. Von Zastrow, Semiconductor Controlled Rectifiers, Prentice-Hall, Englewood Cliffs, N.J., 1964.

[3] Harstad, D.N., "SCR model simplifies computer programs," Electronic Design, Vol. 22, Oct. 25, 1969, pp. 92-95.

[4] Murakami, Y., N. Kosaka, M. Nishimura and N. Sakuma, "A simulation program for thyristor circuits and its applications," Electrical Engineering in Japan, Vol. 91, July - August, 1971, pp. 51-59.

[5] Eisenack H. and H. Hofmeister, "Digitale nachbildung von electrischen netzwerken mit dioden und thyristorem," Archive für Electrotechnik, Vol. 55, November 1972, pp. 32-43.

[6] Revankar, G.N. and S.A. Mahajan, "Digital simulation for mode identification in thyristor circuits," Proc. IEE, Vol. 120, February 1973, pp. 269-272.

[7] Beattie, W.C., W. Monteith, and J.H. Parker, "Analogue modelling of thyristors," Proc. IEE, Vol. 120, No. 7, July 1973, pp. 786-788.

[8] Beattie, W.C. and W. Monteith, "Digital modelling of a thyristor," Proc. IEE, Vol. 120, No. 7, July 1973, pp. 789-790.

[9] Chua, L.O. and P.M. Lin, Computer-Aided Analysis of Electronic Circuits: Algorithms and Computational Techniques, Prentice-Hall, Englewood Cliffs, N.J., 1975.

[10] Chua, L.O. and S.M. Kang, "Section-wise piecewise-linear functions: canonical representation, properties, and applications," Proc. of the IEEE, Vol. 65, June, 1977, pp. 915-929.

[11] Ebers, J.J. and Moll, J.L., "Large signal behavior of junction transistors, Proc. IRE, December 1974, pp. 1761-1772.

[12] Chua, L.O., Nonlinear Circuit Theory, Lecture notes, 1978 European Conference on Circuit Theory and Design, Lausanne, Switzerland, September 4-8, 1978.

[13] Grove, A.S., Physics and Technology of Semiconductor Devices, John Wiley and Sons, New York, 1967.

LIST OF FIGURE CAPTIONS

Fig. 1. (a) A pnpn 4-layer semiconductor device

(b) Symbol of an SCR

(c) A lumped SCR circuit model

Fig. 2. An equivalent SCR circuit model containing only conventional circuit elements (nonlinear capacitors, nonlinear resistors, and linear current-controlled current sources)

Fig. 3. (a) Circuit for simulating the dc SCR anode current I versus the anode-to cathode voltage V, for different values of the gate current I_G.

(b) The dc characteristic curves corresponding to $I_G = 0$, 0.1, and 0.5 mA

Fig. 4. (a) A biased SCR circuit whose V_G-I_G characteristics are being measured

(b) The applied gate voltage waveform $V_G(t)$

(c) The corresponding computed simulated gate current waveform $I_G(t)$

(d) The multivalued V_G-I_G relationship corresponding to $V_G(t)$ and $I_G(t)$

Fig. 5. (a) An SCR circuit for simulating various triggering mechanisms

(b) The applied anode voltage waveform V(t)

(c) The applied gate current waveform $I_G(t)$

(d) The computer-simulated anode current waveform I(t)

Fig. 6. (a) A series RL SCR circuit

(b) The input waveform $v_s(t)$

(c) The triggering pulse train $V_G(t)$

(d) The computer-simulated current I(t)

Fig. 7. (a) A pnpn structure having widths w_{p_1}, w_{n_1}, w_{p_2}, and w_{n_2}, respectively.

(b) Typical doping profile

(c) Depleted charge layers under forwared biased condition

Fig. 8. A symbolic representation of diffusion and recombination current components inside and outside of the depletion regions. Light solid lines depict the flow of holes and dotted lines depict the flow of electrons. Each pair of arrowheads approaching each other denotes a recombined current component.

Fig. A.1 Minority carrier concentration profile in the pnpn structure.

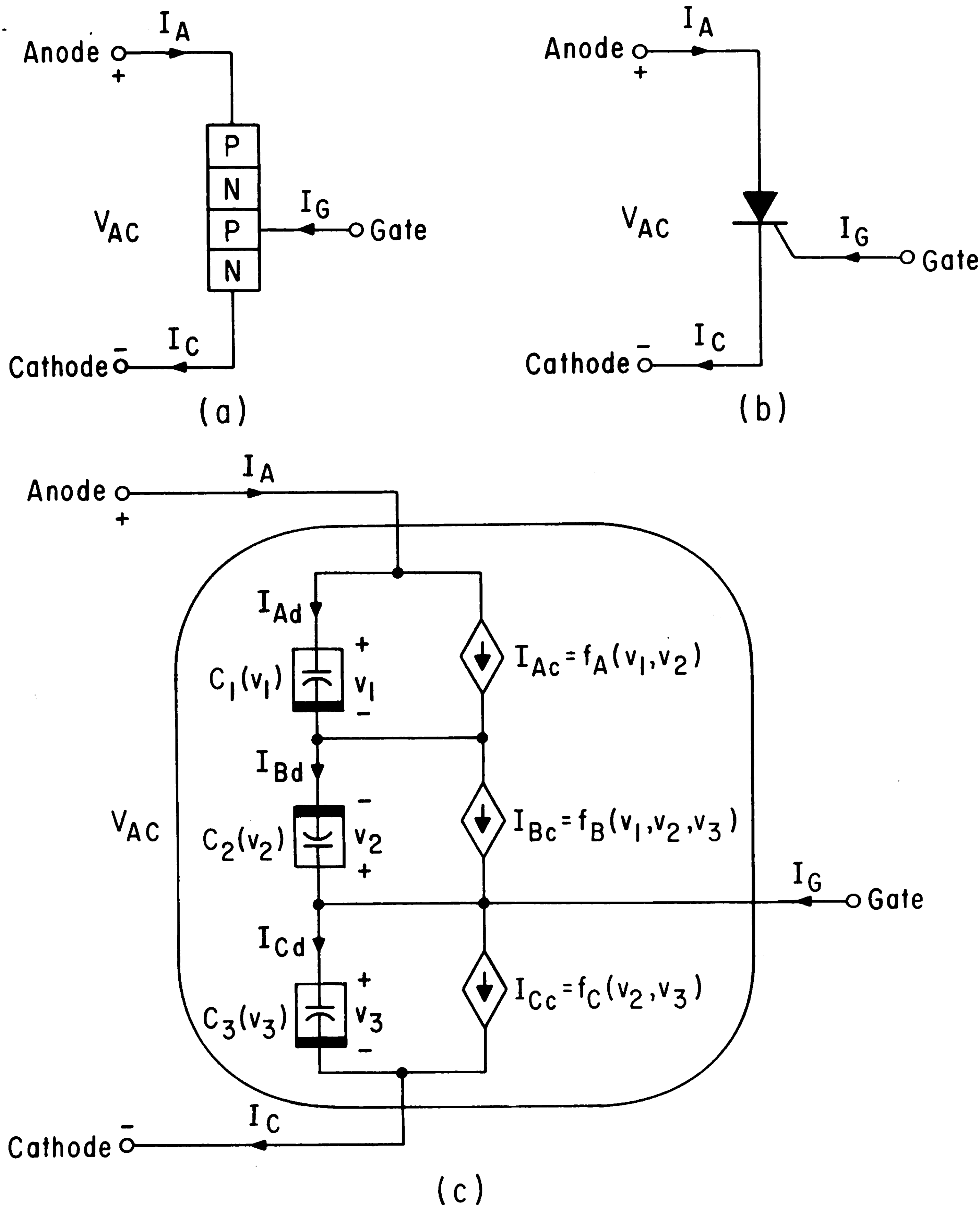

Anode
Cathode
Gate
I_A
I_G
I_C
V_{AC}
P
N
P
N
(a)
(b)
(c)
I_{Ad}
I_{Bd}
I_{Cd}
$C_1(v_1)$
$C_2(v_2)$
$C_3(v_3)$
v_1
v_2
v_3
$I_{Ac} = f_A(v_1, v_2)$
$I_{Bc} = f_B(v_1, v_2, v_3)$
$I_{Cc} = f_C(v_2, v_3)$

Fig. 1

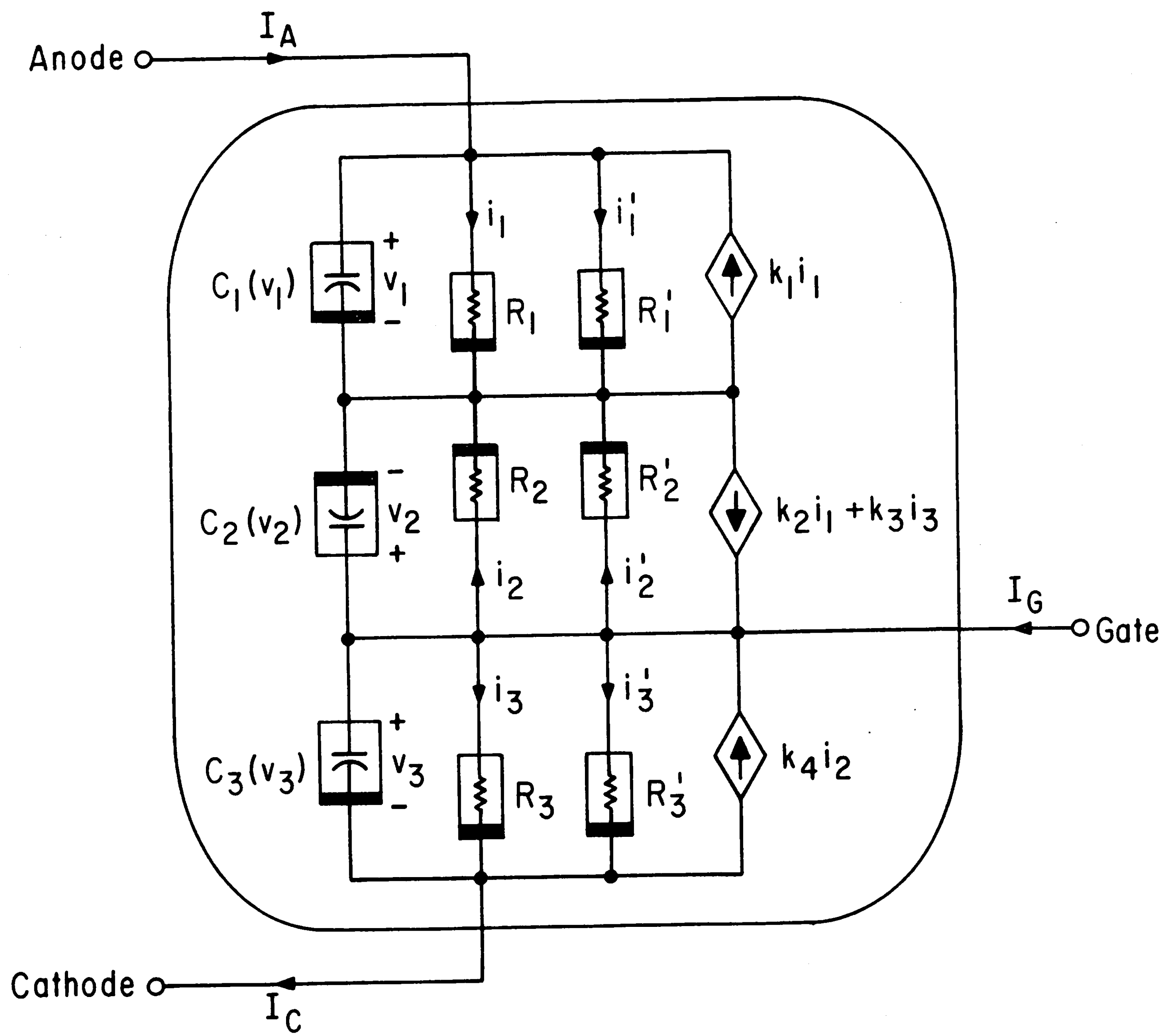

Anode
I_A
i_1
i_1'
$C_1(v_1)$
+
v_1
−
R_1
R_1'
$k_1 i_1$
$C_2(v_2)$
−
v_2
+
R_2
R_2'
$k_2 i_1 + k_3 i_3$
i_2
i_2'
I_G
Gate
i_3
i_3'
$C_3(v_3)$
+
v_3
−
R_3
R_3'
$k_4 i_2$
Cathode
I_C

Fig. 2

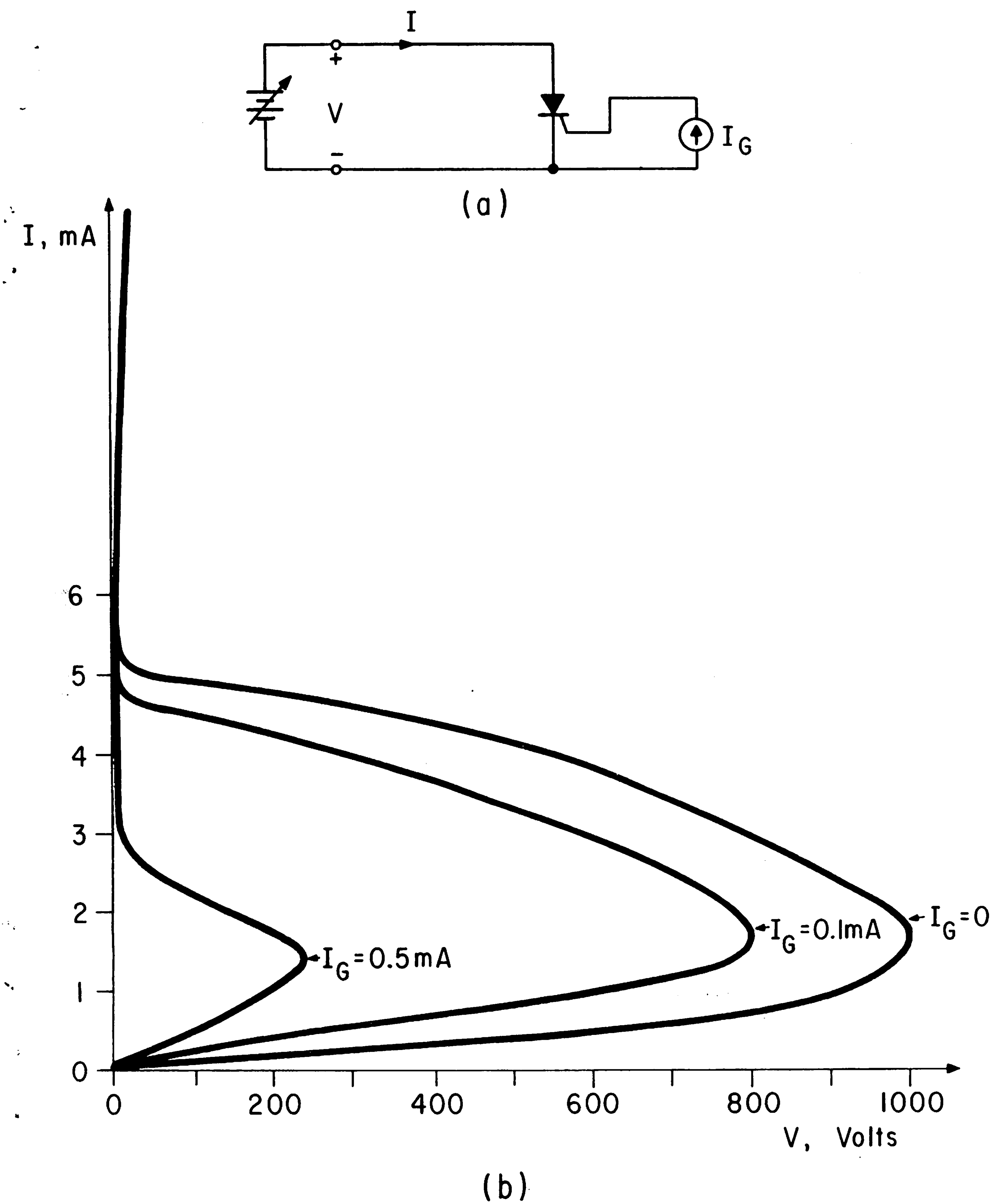

I
+
V
−
I_G
(a)
I, mA
6
5
4
3
2
1
0
0
200
400
600
800
1000
V, Volts
$I_G=0.5mA$
$I_G=0.1mA$
$I_G=0$
(b)

Fig. 3

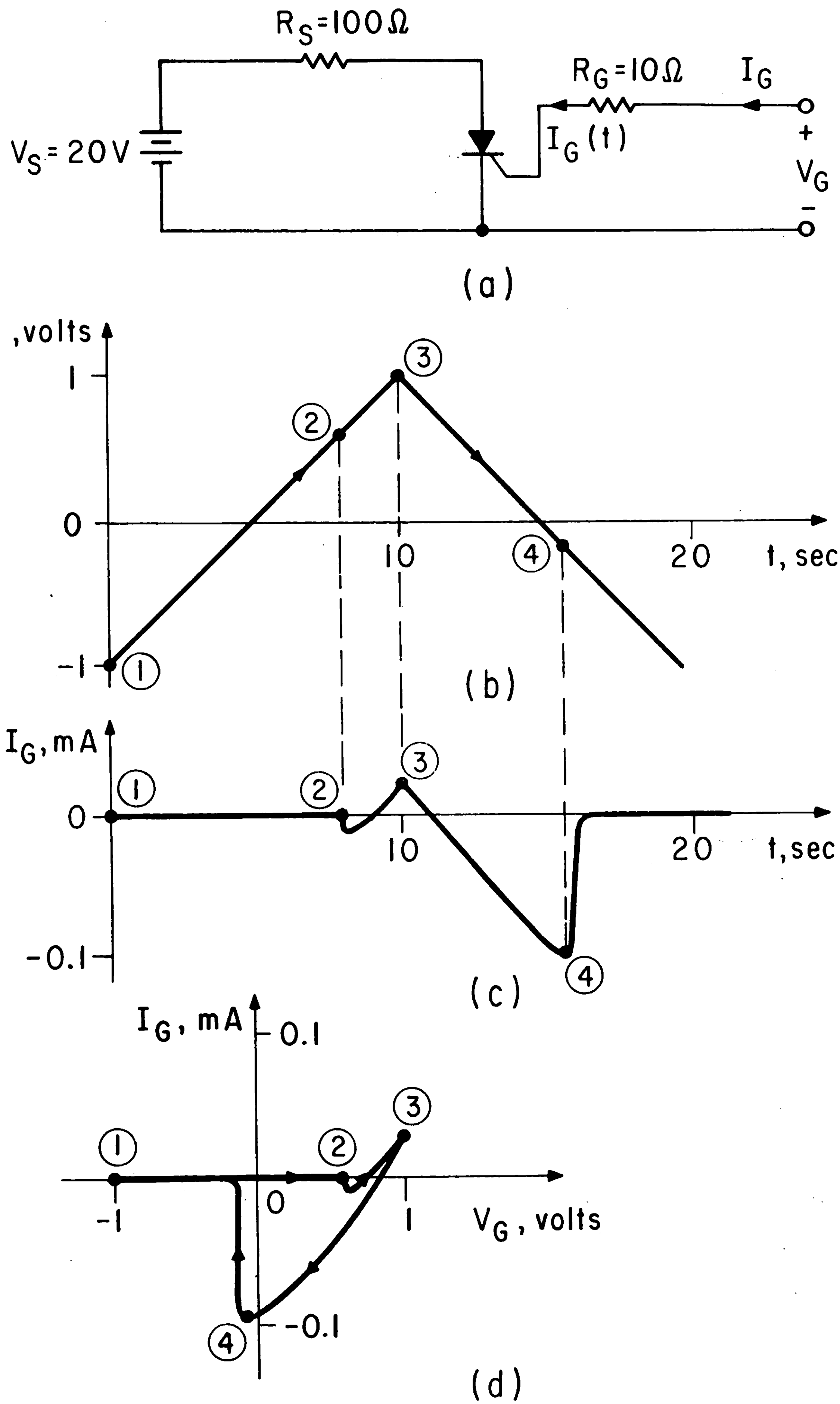

$R_S = 100\Omega$
$R_G = 10\Omega$
I_G
$V_S = 20V$
$I_G(t)$
+
V_G
−
(a)
V_G, volts
1
0
−1
10
20
t, sec
(b)
I_G, mA
0
−0.1
10
20
t, sec
(c)
I_G, mA
0.1
−1
0
1
V_G, volts
−0.1
(d)

Fig. 4

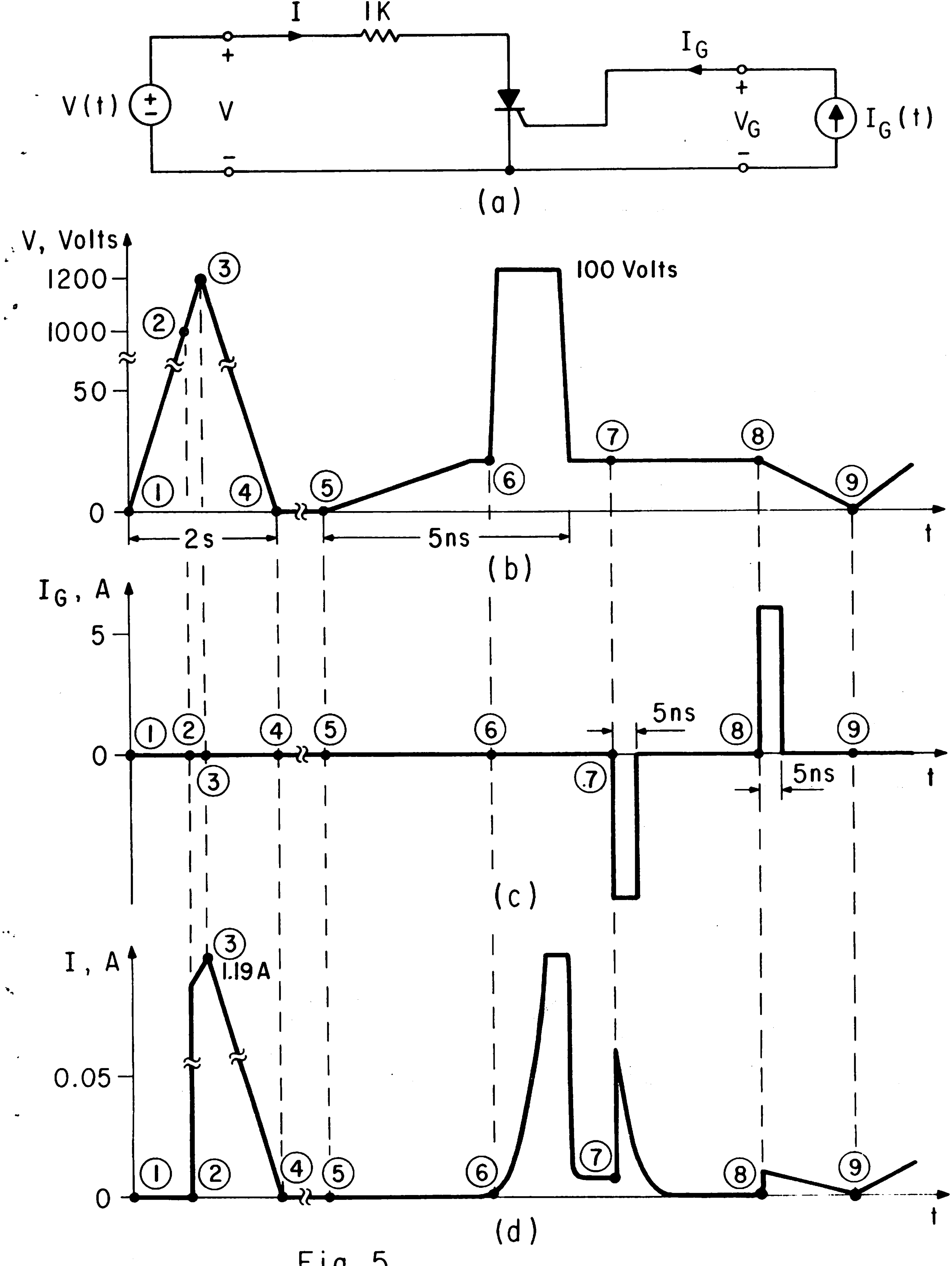

I
1K
I_G
V(t)
+
V
−
+
V_G
−
$I_G(t)$
(a)
V, Volts
1200
1000
50
0
100 Volts
1
2
3
4
5
6
7
8
9
2s
5ns
t
(b)
I_G, A
5
0
5ns
5ns
t
(c)
I, A
1.19A
0.05
0
t
(d)

Fig. 5

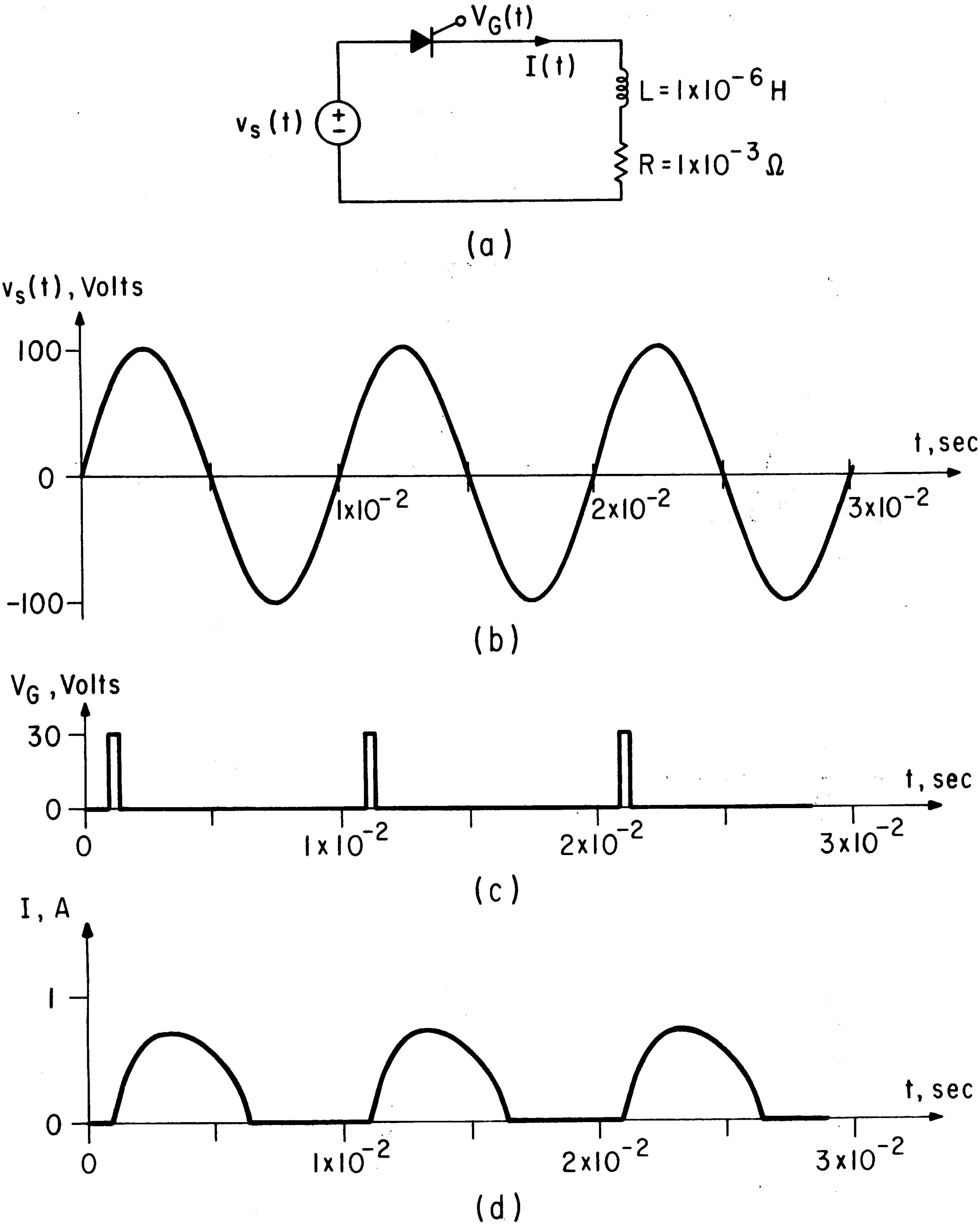

$V_G(t)$
$I(t)$
$L = 1\times10^{-6}$ H
$R = 1\times10^{-3}\,\Omega$
$v_s(t)$
(a)
$v_s(t)$, Volts
100
0
-100
t, sec
1×10^{-2}
2×10^{-2}
3×10^{-2}
(b)
V_G, Volts
30
0
t, sec
0
1×10^{-2}
2×10^{-2}
3×10^{-2}
(c)
I, A
1
0
t, sec
0
1×10^{-2}
2×10^{-2}
3×10^{-2}
(d)

Fig. 6

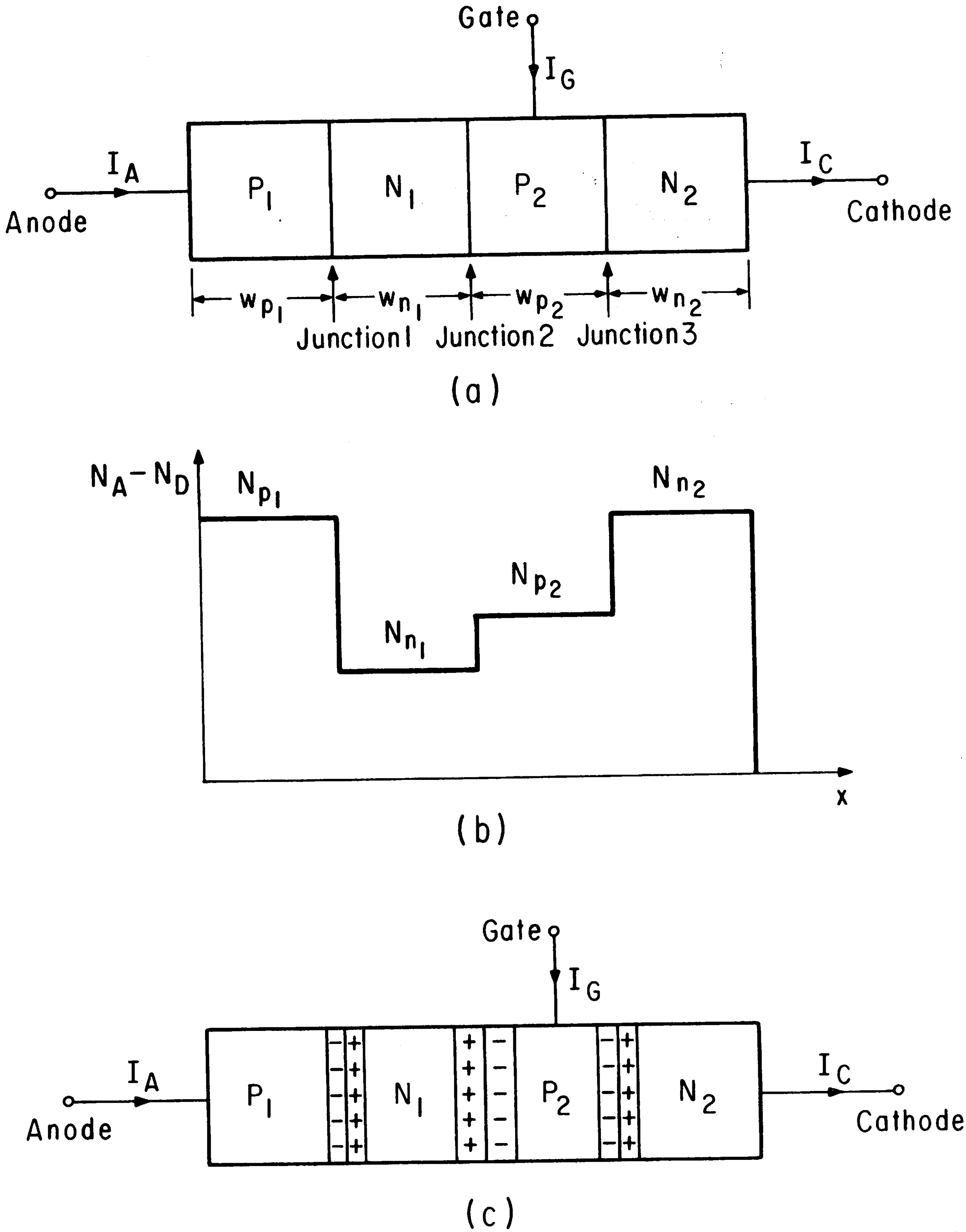
Gate
I_G
I_A
Anode
P_1
N_1
P_2
N_2
I_C
Cathode
w_{p_1}
w_{n_1}
w_{p_2}
w_{n_2}
Junction1
Junction2
Junction3
(a)
$N_A - N_D$
N_{p_1}
N_{n_1}
N_{p_2}
N_{n_2}
x
(b)
Gate
I_G
I_A
Anode
P_1
N_1
P_2
N_2
I_C
Cathode
(c)

Fig. 7

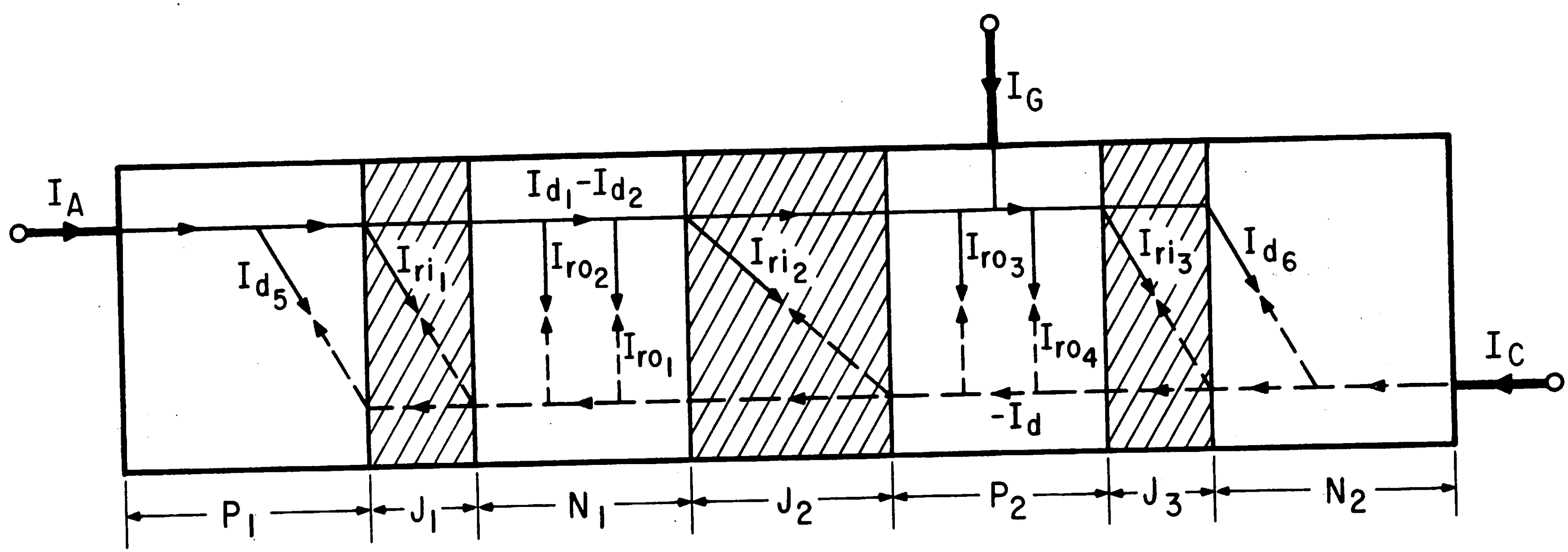

I_A
I_G
I_C
$I_{d_1}-I_{d_2}$
I_{d_5}
I_{d_6}
I_{ri_1}
I_{ri_2}
I_{ri_3}
I_{ro_1}
I_{ro_2}
I_{ro_3}
I_{ro_4}
$-I_d$
P_1
J_1
N_1
J_2
P_2
J_3
N_2

Fig. 8

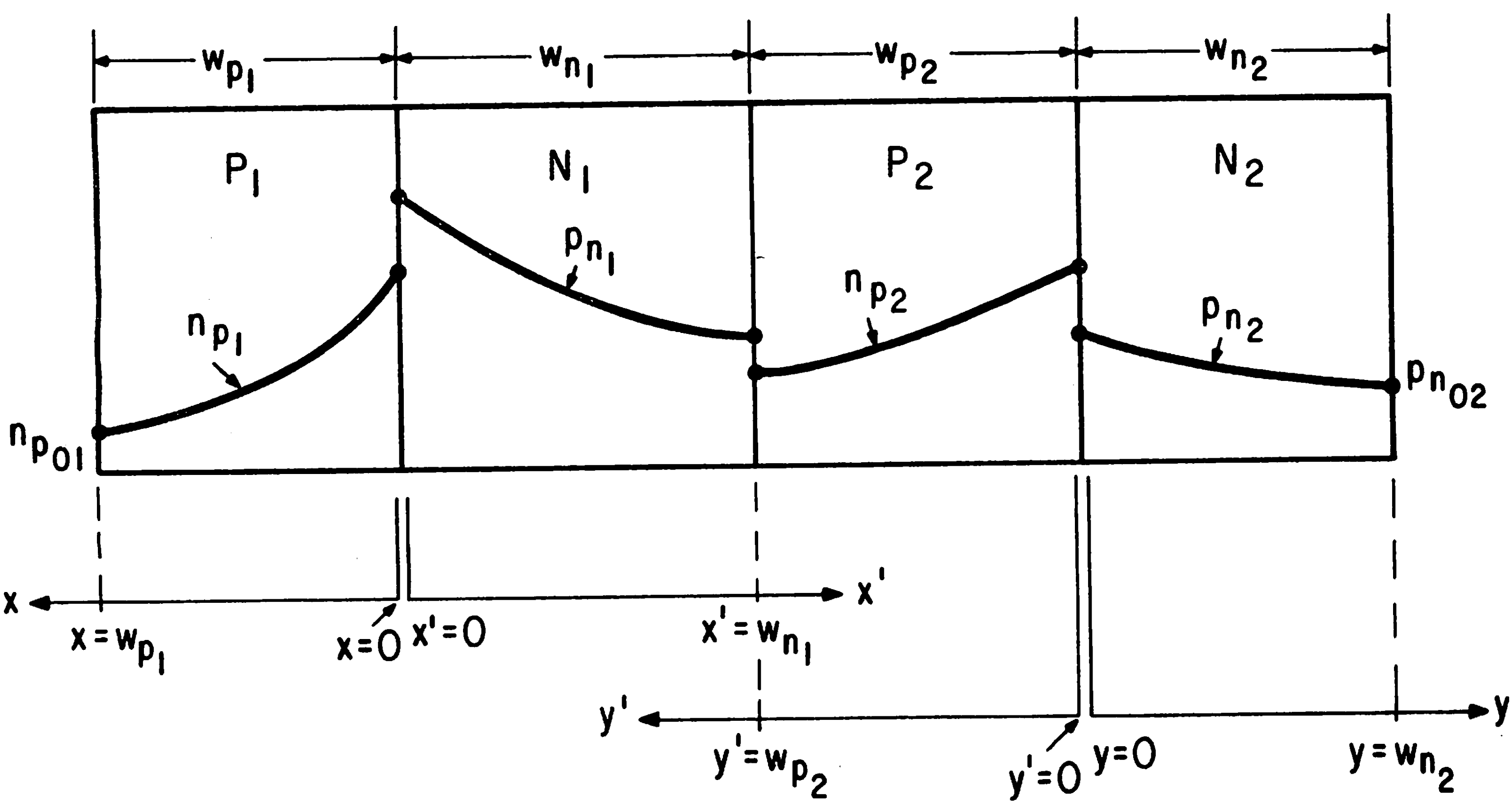

w_{p_1}
w_{n_1}
w_{p_2}
w_{n_2}
P_1
N_1
P_2
N_2
p_{n_1}
n_{p_2}
n_{p_1}
p_{n_2}
$p_{n_{02}}$
$n_{p_{01}}$
x
x'
$x = w_{p_1}$
$x=0$
$x'=0$
$x' = w_{n_1}$
y'
y
$y' = w_{p_2}$
$y'=0$
$y=0$
$y = w_{n_2}$

Fig. A.1